Realistic Conductivity Geometry Model of the Human Head for Interpretation of Neuromagnetic Data

MATTI S. HÄMÄLÄINEN AND JUKKA SARVAS

Abstract—**In this paper, the computational and practical aspects of a realistically-shaped multilayer model for the conductivity geometry of the human head are discussed. A novel way to handle the numerical difficulties caused by the presence of the poorly conducting skull is presented. Using our method, both the potential on the surface of the head and the magnetic field outside the head can be computed accurately. The procedure was tested with the multilayer sphere model, for which analytical expressions are available. The method is then applied to a realistically-shaped head model, and it is numerically shown that for the computation of $\vec{B}$, produced by cerebral current sources, it is sufficient to consider a brain-shaped homogeneous conductor only since the secondary currents on the outer interfaces give only a negligible contribution to the magnetic field outside the head. Comparisons with the sphere model are also included to pinpoint areas where the homogeneous conductor model provides essential improvements in the calculation of the magnetic field outside the head.**

I. Introduction

In the last few years, the magnetic fields arising from electrical currents in the human brain have been subject to increasing interest [1], [2]. The proven ability of the neuromagnetic measurements to reveal new aspects of the brain function has caused a drive for better instruments and for more effective means of analyzing the data.

A key question in the analysis is the inverse problem: what can we say about the underlying electrical currents, associated with neural activity, on the basis of neuromagnetic measurements plus the extra knowledge one has about the brain? Up to now, the study of the inverse problem has resorted to crude simplifications. Especially, the head has been modeled with a sphere approximating the local inner curvature of the skull. Considering the complex shape of this surface, it is evident that the assumption of sphericity is poor when temporal and frontal areas are studied or when measurements cover a large area on the head. For this reason, new efforts are in progress to explore the limitations of the sphere model and to find practical ways to refine the model where necessary [3], [4].

The starting point of this paper is the usual integral equation method of calculating the magnetic field produced by electrical currents in an arbitrarily-shaped piecewise homogeneous conductor [5], [6]. However, in the case of the brain, the poorly conducting skull causes difficulties in obtaining accurate results numerically without excessive amount of computation time. In this paper, a new and numerically effective solution, arising from the physical constraints involved, is presented. It is also shown that the algorithm is accurate and computationally practicable. Since our calculation involves the potential on the surface of the head, a numerical solution for the EEG forward problem is automatically included.

We have previously suggested [7] that, for the computation of neuromagnetic fields arising from cortical sources, it is sufficient to replace the skull by a perfect insulator and, therefore, to model the head as a bounded brain-shaped homogeneous conductor. In this paper, we directly verify this proposal by comparing the fields calculated using the homogeneous and multilayer models. Since the former model is applicable even to on-line analysis, this result provides a valuable tool to handle those cases in which the sphere model is inadequate.

II. The Integral Equations

A reasonable approximation for the conductivity geometry of the human head is a piecewise homogeneous conductor. The interfaces between the regions of different conductivity will be denoted by $S_1, \cdots, S_m$, with S_1 circumventing all the remaining surfaces, i.e., S_1 is the surface of the scalp. It can be shown [5], [8] that the electric potential V at $\vec{r} \in S_i$ obeys the integral equation

$$(\sigma_i^- + \sigma_i^+)V(\vec{r}) = 2V_0(\vec{r}) + \frac{1}{2\pi}\sum_{j=1}^{m}(\sigma_j^- - \sigma_j^+) \cdot \int_{S_j} V(\vec{r}')\, d\Omega_{\vec{r}}(\vec{r}') \qquad (1)$$

where $V_0(\vec{r})$ is the potential caused by the current source in an infinite homogeneous medium with $\sigma = 1$. The conductivities inside and outside S_j are denoted by σ_j^- and σ_j^+, respectively. The solid angle subtended at $\vec{r}$ by a surface element $\vec{dS}$ at $\vec{r}'$ is denoted by $d\Omega_{\vec{r}}(\vec{r}')$ and it is given by

$$d\Omega_{\vec{r}}(\vec{r}') = \frac{\vec{r}' - \vec{r}}{|\vec{r}' - \vec{r}|^3} \cdot \vec{dS_j}(\vec{r}'). \qquad (2)$$

Manuscript received June 17, 1987; revised September 12, 1988. This study was finacially supported by the Academy of Finland.

The authors are with Low Temperature Laboratory, Helsinki University of Technology, SF-02150 Espoo, Finland.

IEEE Log Number 8825089.

For the numerical solution of (1), the surfaces S_i are divided into suitable triangles $\Delta_1^i, \cdots, \Delta_{n_i}^i$ resulting in a set of linear equations [9]:

$$V^i = \sum_{j=1}^{m} B^{ij} V^j + g^i; \qquad i = 1, \cdots, m \tag{3}$$

where V^i and g^i are column vectors and B^{ij} are matrices whose elements are defined by

$$V_k^i = \frac{1}{\mu_k^i} \int_{\Delta_k^i} V(\vec{r}\,)\, dS_i, \tag{4}$$

$$g_k^i = \frac{1}{\mu_k^i} \frac{2}{\sigma_i^- + \sigma_i^+} \int_{\Delta_k^i} V_0(\vec{r}\,)\, dS_i, \quad \text{and} \tag{5}$$

$$B_{kl}^{ij} = \Gamma_{ij} \frac{1}{\mu_k^i} \frac{1}{2\pi} \int_{\Delta_k^i} \Omega_{\Delta_l^j}(\vec{r}\,)\, dS_i, \tag{6}$$

respectively. Here μ_k^i is the area of the kth triangle Δ_k^i on the surface S_i and $\Omega_{\Delta_l^j}(\vec{r}\,)$ is the solid angle subtended by Δ_l^j at $\vec{r}$. For $k = l$ and $i = j$ we must set $\Omega_{\Delta_l^j}(\vec{r}\,) = 0$. The number of triangles on each surface S_j is denoted by n_j and $\Sigma_{j=1}^m n_j = N$. The multipliers Γ_{ij} are given by

$$\Gamma_{ij} = \frac{\sigma_j^- - \sigma_j^+}{\sigma_i^- + \sigma_i^+}. \tag{7}$$

In practice, the elements B_{kl}^{ij} are computed by replacing $\Omega_{\Delta_l^j}(\vec{r}\,)$ on Δ_k^i by its value at the centroid $\vec{c}_k^{\,i}$ of the triangle. Using this approximation we get $B_{kl}^{ij} \simeq \Gamma_{ij} \Omega_{\Delta_l^j}(\vec{c}_k^{\,i})/2\pi$. The solid angle subtended by a triangle at a point can be calculated from the analytical formula given by Barnard *et al.* [10]. Even with this simplification, the calculation of the matrix elements B_{lk}^{ij} is the most time consuming part of the numerical solution for the potentials. However, the solid angles depend only on the conductor geometry, allowing $\Omega_{\Delta_l^j}(\vec{c}_k^{\,i})$ to be precalculated if the geometry is kept fixed and only the conductivities and the source structure are changed.

Since the potential is defined only up to an additive constant, (3) has no unique solution. This ambiguity can be removed by deflation [10], which means that B^{ij} must be replaced by

$$C^{ij} = B^{ij} - \frac{1}{N} e_i e_j^T \tag{8}$$

where e_i is a vector with all its n_i components equal to one and T denotes the transpose. The deflated equations

$$V^i = \sum_{j=1}^{m} C^{ij} V^j + g^i; \qquad i = 1, \cdots, m \tag{9}$$

possess a unique solution which is also a solution for the original (3). Equation (9) is most conveniently solved by iterative algorithms; we have employed the Gauss–Seidel iteration. The speed of convergence can be increased by applying a multiple deflation [9]. In our case the rate of convergence is improved at best by a factor of two by this method. For the subsequent treatment it is sufficient to consider the single deflation only.

Once the solution for the potential is known, the magnetic field at a given point can be obtained from the Geselowitz' formula [6]:

$$\vec{B}(\vec{r}\,) = \vec{B}_0(\vec{r}\,) + \frac{\mu_0}{4\pi} \sum_{j=1}^{m} (\sigma_j^- - \sigma_j^+) \cdot \int_{S_j} V(\vec{r}\,') \frac{\vec{r} - \vec{r}\,'}{|\vec{r} - \vec{r}\,'|^3} \times \vec{d}S_j, \tag{10}$$

which gives the magnetic field for all $\vec{r}$ not on any of the surfaces S_j. Here $\vec{B}_0(\vec{r}\,)$ is the magnetic field produced by the primary current sources in an infinite homogeneous medium and the second term is the contribution of the volume currents which is seen to be equal to the magnetic field of a surface current distribution on S_js, often referred to as the secondary currents. Having the potential values at the centroids of the triangles Δ_k^i, we approximate the integral in the second term of (10) by

$$\int_{S_j} V(\vec{r}\,') \frac{\vec{r} - \vec{r}\,'}{|\vec{r} - \vec{r}\,'|^3} \times \overrightarrow{dS_j} \simeq \sum_{k=1}^{n_j} V_k^j \int_{\Delta_k^j} \frac{\vec{r} - \vec{r}\,'}{|\vec{r} - \vec{r}\,'|^3} \times \overrightarrow{dS_j}. \tag{11}$$

In the case of the head it is sufficient to consider three layers: the brain, the skull, and the scalp. Thus, in the following $m = 3$, and S_1, S_2, and S_3 are the scalp–air, skull–scalp, and brain–skull interfaces, respectively. The scalp and the brain have almost equal conductivities while the conductivity of the skull is about a hundred times smaller. The ratio of the conductivity of the skull to the conductivity of the brain will be denoted by β and it will be assumed that $\sigma_{\text{brain}} = \sigma_{\text{scalp}} = \sigma_0$. From these assumptions it follows that only the source terms g^i will depend on σ_0 and we have $g^i \propto 1/\sigma_0$ and, consequently, $V^i \propto 1/\sigma_0$. It is also readily seen that $\vec{B}(\vec{r}\,)$ in (10) is independent of σ_0.

III. The Modified Equations

It has been previously shown [4] that an accurate numerical solution of (1) via (3), or its deflated versions, is difficult to obtain if β is small, say $\beta < 0.1$. The reasons for this difficulty are now explained and a method to remove them is presented.

As β tends to zero, the solution of the integral equations corresponding to (3) approaches the solution of the equation for the bounded homogeneous conductor on S_3 and vanishes on the remaining surfaces. The behavior of V as $\beta \to 0$ is not, however, accurately reproduced by the discretized equations. If $\beta \ll 1$, V^1 and V^2 are much smaller in magnitude than V^3. Accordingly, in the third equation of (9)

$$V^3 = C^{33} V^3 + g^3 + \left\{ \sum_{j=1}^{2} C^{3j} V^j \right\} \tag{12}$$

the terms in braces involving V^1 and V^2 are small and the accuracy of V^3 is not greatly affected by the small value of β. However, the situation is quite different for V^1 and V^2. Since V^3 is almost independent of V^1 and V^2, we may consider it as a part of the source term

$$V^i = \sum_{j=1}^{2} C^{ij} V^j + \{ g^i + C^{i3} V^3 \}, \qquad i = 1, 2. \quad (13)$$

The numerical difficulty is that the effective source term $g^i + C^{i3}V^3$ is composed of two comparatively large parts which should cancel as $\beta \to 0$, as (19) of the Appendix shows. Since V^3 is calculated numerically, we can expect a high relative error in the sum $g^i + C^{i3}V^3$ for small β.

However, the numerical problem is removed if the solution is sought in the form

$$V^i = W^i + W_0^i \quad (14)$$

where $W_0^1 = W_0^2 = 0$ and W_0^3 is the potential on the surface of a homogeneous conductor bounded by S_3. It turns out, see the Appendix, that the discretized equations for the unknown functions W^i are

$$W^i = \sum_{j=1}^{m} C^{ij} W^j + \sigma_3^+ h^i \quad (15)$$

where h^i is a new source term defined by

$$h^1 = g^1/\sigma_3^-, \quad h^2 = g^2/\sigma_3^-,$$
$$h^3 = g^3/\sigma_3^- - \frac{2}{(\sigma_3^- + \sigma_3^+)} W_0^3. \quad (16)$$

While studying the modified equations we found that the potentials V^1, V^2, and V^3 can now be computed accurately for all values of β. Note that (15) is not exactly equivalent to the original discretized (9) since the physical constraints described by

$$\frac{2V_0(\vec{r})}{\sigma_3^-} + \frac{1}{2\pi} \int_{S_3} W_0(\vec{r}\,')\, d\Omega_{\vec{r}}(\vec{r}\,') = \begin{cases} W_0(\vec{r}) & \text{if } \vec{r} \in S_3 \\ 0 & \text{if } \vec{r} \in S_1, S_2 \end{cases} \quad (17)$$

were used to derive (15), see the Appendix. From the computational point of view the addition of these constraints means that an extra matrix inversion to find W_0^3 is required. This is not, however, a serious drawback since the extra time involved is short compared with the time which would be needed if the number of triangles on the surfaces S_j is increased in order to reach a reasonable accuracy with (9). Meijs *et al.* [4] have previously estimated that, in order to obtain 5 percent accuracy for the solution of (9), the number of triangles must be of the order of 10^4. The time complexity of the Gauss–Seidel algorithm is at least $O(N^2)$ since each iteration loop requires N^2 multiplications. So for the case of 10^4 triangles this number will be of the order of 10^8. On the other hand, it will be shown that with (15) one-percent accuracy on the outer layers can be reached with only 300 triangles/surface. With this number of triangles the time complexity of our algorithm is $O((3 \cdot 300)^2 + 300^2)$ which is about two orders of magnitude smaller than the time required for the direct solution with (9).

IV. Results

A. Spherically Symmetric Conductor

The accuracy of the multilayer model was tested with a spherically symmetric conductor. The numerical solution of (1), with $m = 3$, was compared with the values given by analytical expressions available for the layered sphere model [11].

The radii of the spherical interfaces were chosen to be 90, 95, and 100 mm. The two outer spheres were divided into 280 triangles, and 280 or 360 triangles were used on the innermost sphere. The current source was a dipole ($Q = 10$ nA) parallel to the xy plane on the z axis. The depth of the dipole was varied between 20 and 40 mm from the scalp. Since the source was near the surface, the potential changes more rapidly as a function of location near the dipole than on the opposite side of the sphere. Therefore, the triangles were distributed unevenly with 2/3 of the triangles on the hemisphere containing the dipole.

To demonstrate the inaccuracy of (9) and the improvement provided by the modification described in (14)–(16), we compared the two numerical solutions with the analytical calculation when β was gradually decreased from 0.5 to 0.01. It was observed that both the direct and modified numerical solution methods gave correctly shaped potential patterns. However, the peak values given by the direct method were too large on the outer surfaces (the error being 10 percent at $\beta = 0.1$ and 35–40 percent at $\beta = 0.01$). On the innermost surface the relative error at the potential peak was 5–6 percent for 280 triangles on the surface and 2–4 percent for 360 triangles. The error on the innermost surface did not show significant dependence on β. The values quoted here are for a dipole at 30 mm depth from the surface of the outermost sphere.

Applying the modified method, the relative error on the outer surfaces dropped below 7 percent at $\beta = 0.1$ and below 4 percent at $\beta = 0.01$. A summary of the relative errors for the modified method at the potential peaks for various source depths and conductivities is given in Table I.

After having shown that the electric potential can be accurately computed, we proceeded to integrate the magnetic field according to (10) and (11). Again, analytical expressions for all components of $\vec{B}$ are available [12], [13]. Comparison of the numerically calculated field values with those given by the exact analytical expressions showed that the shape of the field pattern is almost correct. The fields at the extrema differed more from the correct values for the tangential field components (B_θ, B_ϕ) than for the radial component (B_r). This is due to the fact that B_r receives no contribution from the (radial) secondary currents and thus the errors in potential values con-

TABLE I
COMPARISON OF THE NUMERICALLY CALCULATED POTENTIALS WITH THE ANALYTICAL VALUES FOR A SPHERICAL CONDUCTOR. THE RELATIVE ERRORS AT THE POTENTIAL MAXIMA ON SURFACES S_1, S_2, AND S_3 ARE GIVEN IN COLUMNS LABELED WITH r_1, r_2, AND r_3, RESPECTIVELY

Depth/mm	β	r_1/%	r_2/%	r_3/%
20	0.1	6.4	6.7	-2.0
	0.05	7.5	7.5	-2.5
	0.01	2.9	3.5	-2.1
30	0.1	-2.5	-1.8	2.5
	0.05	-1.5	-1.0	2.5
	0.01	1.8	2.8	2.3
40	0.1	-0.6	-0.2	0.1
	0.05	0.2	1.3	0.2
	0.01	0.2	-0.4	-1.1

TABLE II
COMPARISON OF THE NUMERICALLY CALCULATED MAGNETIC FIELD WITH THE ANALYTICAL VALUES FOR A SPHERICAL CONDUCTOR. THE RELATIVE ERRORS AT THE PEAKS OF THE THREE-FIELD COMPONENTS GIVEN IN COLUMNS LABELED $r(B_r)$, $r(B_\theta)$, AND $r(B_\phi)$, RESPECTIVELY.

Depth/mm	β	$r(B_r)$/%	$r(B_\theta)$/%	$r(B_\phi)$/%
20	0.1	2.0	1.8	-0.9
	0.05	1.9	1.3	0.03
	0.01	1.6	1.0	1.3
30	0.1	0.9	6.1	4.9
	0.05	0.8	5.9	4.8
	0.01	0.6	5.9	5.0
40	0.1	0.02	6.5	5.9
	0.05	-0.03	5.9	5.7
	0.01	-0.05	5.3	5.7

tribute only through the small deviation of the triangle normals from the radial direction. Since secondary currents contribute to B_θ and B_ϕ, these components will be affected by both the geometrical inaccuracies and by the errors in potential values. The results summarized in Table II show that the magnetic field is computed with better than 7 percent accuracy for all source depths and β values shown.

B. Construction of the Realistically-Shaped Model

An essential goal of this work is to apply the methods described in the two previous sections to a conductor which closely approximates the actual shape of the head. The surfaces S_1, S_2, and S_3 should take the form of the scalp–air, the skull–scalp, and the skull–brain interfaces, respectively. Here we have to tackle two problems which are not present in the analytically solvable sphere model: 1) the shape of the surfaces is not readily available and 2) the accuracy of the results is more difficult to verify.

We approached the first problem by measuring the shape of the skull's inner surface from an anatomically accurate model (manufactured by Somso, FRG). The surface was manually divided into triangles whose area was approximately 2 cm^2. Smaller triangles were used on the bottom of the skull where the surface is more convoluted. The distances to the vertices of the triangles were measured from three fixed points with a pair of compasses. From these measurements the rectangular coordinates of the vertices were computed. The horizontal plane about 5 cm above the eyes where the skull had been cut into two halves was used as the xy plane. The origin of the coordinate system was the approximate center of gravity of this cross section with the y axis in the sagittal plane. The resulting net of 406 triangles is shown in perspective view in Fig. 1.

We approximated the shapes of S_1 and S_2 from the shape of S_3 using a 5 mm thickness for the skull and the scalp. This is justified since the potentials on S_1 and S_2 are much smaller than those on S_3 and yield only minor contributions to the magnetic field which is in practice measured at least 15 mm above the head.

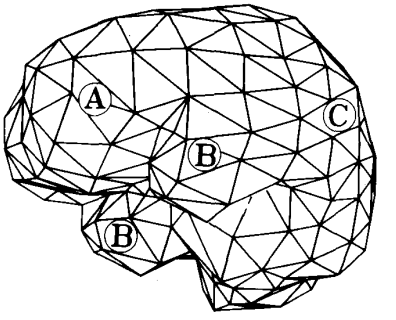

Fig. 1. A perspective view of the triangle net on the inner surface of the skull (S_3). The encircled capital letters indicate the location of the frontal lobe (A), the temporal lobes (B), and the occipital lobe (C), respectively. Notice the irregular shape of the bottom of the skull in the frontal areas.

The same information, here found by studying a plastic model, could also have been obtained from high quality CT or NMR scans. However, since the results shown here were not used for interpretation of measurements on an actual subject, the use of the plastic model was convenient.

The accuracy of the electric potential and magnetic field calculations cannot be easily verified in the case of an arbitrarily shaped conductor. An obvious way to proceed would be to increase the density of the triangles gradually and show that the results approach some limiting value. Then an appropriate number of triangles could be chosen to reach a given accuracy. This method needs, however, a lot of computing time and one can, indeed, make reasonable estimates of accuracy without having to repeat the calculations with a very large number of triangles. An upper limit for the discretization error when the electric potential is computed is $K\rho^{\gamma - 1/5}$ [14] where K is some constant, ρ is the maximum of the diameters of the triangles Δ_i^k, and $0 < \gamma \leq 1$ is a constant depending on the curvature of S_i. Since the sphere model dimensions were chosen close to those of the head, we expect that even for the

head shaped conductor the magnetic field is obtained with about 5 percent accuracy.

C. Comparisons Between Various Models

In this section the multilayer head model is compared with two simpler models: the homogeneous model and the sphere model. The homogeneous model sets $\beta = 0$, leaving only (17) to be solved while the sphere model assumes that the conductor is spherically symmetric with the center chosen to give a good fit between a sphere at the origin and the skull's inner surface above the source. In practice, the origin was determined by drawing two perpendicular cross sections of the triangulation representing the inner surface of the skull and by manually fitting circles to these cross sections. The average location of these two circle origins was then used as the center of symmetry for the sphere model.

A total of four different areas for the source location were chosen (Fig. 2). Qualitative differences of the skull's shape between these regions can be summarized as follows:

1) The occipital area. Here the shape of the head is almost spherical and no significant differences should be found unless the sources are in deep locations.

2) The posterotemporal area. The assumption of sphericity is slightly violated since the radius of curvature is larger on the $z = 0$ cross section than in the perpendicular direction. A compromize must be made between these two clearly distinct values.

3) The frontotemporal area. The bottom of the skull has a complicated nonspherical shape in front of the temporal lobe. It is difficult to find any sphere which even roughly approximates the real shape.

4) The frontal area. The upper part of the skull is roughly spherical while the bottom of the skull is essentially flat. Again, fitting a sphere to this shape is ambiguous.

In each area (see Fig. 2) at least five different source depths were studied. The 10 nA dipoles were perpendicular to the normal of the brain surface and parallel to the xz plane. As shown, two source levels were chosen in the frontal area in order to see the effects of the proximity of the flat bottom of the skull. The depth d of the sources, measured from the surface of the brain, ranged between 10 and 60 mm.

The three components of the magnetic field were computed for each source on spherical surfaces at 15 mm distance from the scalp using all the three conductor model candidates: the multilayer model, the homogeneous model, and the sphere model. Usually $\beta = 0.01$ for the multilayer model, but some tests were made with $\beta = 0.5, 0.1$, and 0.05. The three models agreed for all sources close to the brain surface ($d \leq 20$ mm).

In the occipital area the results are still quite similar up to 40 mm depth. For deeper sources the homogeneous model and the multilayer model agree but the distance between the extrema of B_r is smaller than the sphere model would predict. The B_ϕ and B_θ patterns are also of similar

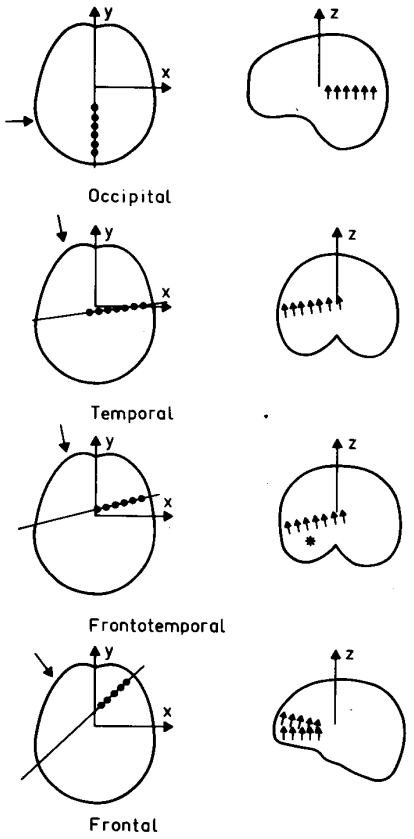

Fig. 2. Cross sections of the brain showing the locations of the test dipoles. Left: cross section $z = 0$. The viewing direction is indicated by the arrows. Right: cross sections parallel to the z axis through the lines drawn in the left column.

shape but the sphere model gives from 10 to 30 percent too small amplitudes when the source depth was larger than 20 mm. For temporal sources, the distance between the B_r extrema in the sphere model was about 10 percent too large at $d = 40$ mm and 20 percent too large at $d = 60$ mm. It must be pointed out, however, that the amplitude of B_r produced by a 60 mm deep 10 nA dipole is about 10 ft, which is quite small compared to the corresponding value of 330 ft given by a 10 mm deep dipole.

Clear differences between the conductor models were found in the frontotemporal and frontal regions where $d > 20$ mm, and with sources in the lower position close to the irregularly-shaped bottom of the skull. In addition to changes in field amplitudes and distances between extrema, distortions of the shape of the field patterns were found. As an illustrative example of the choice of the conductor model, a comparison for a 25 mm deep frontotemporal dipole (see Fig. 2) is shown in Figs. 3–5. It is seen that, although the shape of the field pattern is distorted when the sphere model is replaced by one of the realistically shaped models, the homogeneous model still agrees with the multilayer model indicating that the former is capable of predicting accurately all components of the magnetic field.

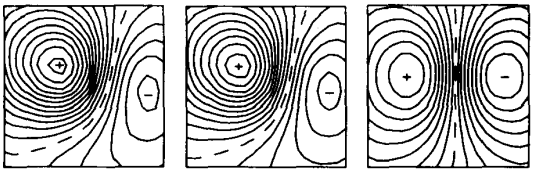

Fig. 3. The radial component of the magnetic field (B_r), produced by a 25 mm deep dipole in the frontotemporal area (marked with an asterisk in Fig. 2) at 15 mm distance from the scalp. Left: The multilayer model. Middle: The homogeneous model. Right: The sphere model. Difference between the contour lines is 10 ft.

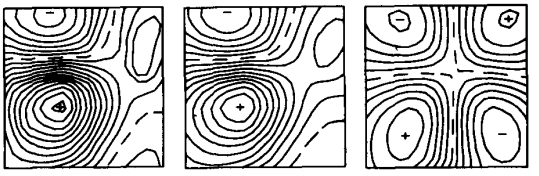

Fig. 4. As Fig. 3, but for the B_θ component. Difference between the contour line is 5 ft.

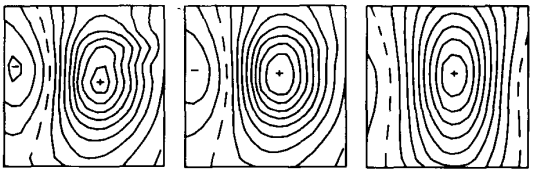

Fig. 5. As Fig. 3, but for the B_ϕ component. Difference between the contour lines is 10 ft.

V. Conclusions

The present work introduces a method to avoid the numerical inaccuracies found in applying the discretized integral equation method for computation of the electric potentials and the magnetic fields produced by cerebral current sources. The method was tested with a spherically symmetric conductor. Its application to a realistic head-shaped conductor showed that the sphere model is not accurate enough for computing the magnetic fields of deep sources or sources near the bottom of the skull in frontotemporal and frontal areas. However, even in these cases the agreement of the homogeneous conductor model and the multilayer model is good. This suggests that, for accurate computation of magnetic fields produced by sources in the frontal and frontotemporal areas, the brain shaped homogeneous conductor model should be applied. For the study of other cortical areas the use of the sphere model, when correctly applied, is sufficient.

Appendix

This Appendix describes a method to remove the numerical inaccuracy caused by the low conductivity of the skull, in the solution of the discretized integral (9).

Let $W_0(\vec{r})$ be a solution of the integral equation for the homogeneous conductor G (conductivity $\sigma = \sigma_m^-$) bounded by S_m:

$$W_0(\vec{r}) = \frac{2V_0(\vec{r})}{\sigma_m^-} + \frac{1}{2\pi}\int_{S_m} W_0(\vec{r}')\, d\Omega_{\vec{r}}(\vec{r}'), \quad \vec{r} \in S_m. \tag{18}$$

If $\vec{r} \notin G$ we can take $W_0(\vec{r}) = 0$. With help of the Green's second indentity, it is then easy to show that

$$\frac{2V_0(\vec{r})}{\sigma_m^-} + \frac{1}{2\pi}\int_{S_m} W_0(\vec{r}')\, d\Omega_{\vec{r}}(\vec{r}') = 0, \quad \text{if } \vec{r} \notin G. \tag{19}$$

Next, we decompose $V(\vec{r})$ as $V(\vec{r}) = W(\vec{r}) + W_0(\vec{r})$. That is, $V(\vec{r})$ is the solution for the homogeneous conductor plus a correction term $W(\vec{r})$. Inserting this decomposition and (18) and (19) into (1) we obtain

$$(\sigma_i^- + \sigma_i^+)W(\vec{r}) = 2\sigma_m^+ X(\vec{r}) + \frac{1}{2\pi}\sum_{j=1}^{m}(\sigma_j^- - \sigma_j^+) \cdot \int_{S_j} W(\vec{r}')\, d\Omega_{\vec{r}}(\vec{r}') \tag{20}$$

which is identical to (1), except for the source term $\sigma_m^+ X(\vec{r})$, which is given by

$$X(\vec{r}) = \begin{cases} 2V_0(\vec{r})/\sigma_m^- - 2W_0(\vec{r}) \\ \quad \text{if } \vec{r} \in S_m \\ 2V_0(\vec{r})/\sigma_m^- \\ \quad \text{if } \vec{r} \in S_1, \cdots, S_{m-1}. \end{cases} \tag{21}$$

Since (1) and (20) are are identical, except for the source term, we readily obtain the deflated discrete version of (20):

$$W^i = \sum_{j=1}^{m} C^{ij}W^j + \sigma_m^+ h^i; \quad i = 1, \cdots, m. \tag{22}$$

Here, the kth element of W^i is an average of $W(\vec{r})$ over the kth triangle on S_i:

$$W_k^i = \frac{1}{\mu_k^i}\int_{\Delta_k^i} W(\vec{r})\, dS_i \tag{23}$$

and h^i is the modified source vector on S_i, related to the original source vector g^i by

$$h^i = g^i/\sigma_m^-, \quad i = 1, \cdots, m-1,$$
$$h^m = g^m/\sigma_m^- - \frac{2}{(\sigma_m^- + \sigma_m^+)}W_0^m. \tag{24}$$

Note that, to be able to compute h^m, it is necessary to know W_0^m which is the solution of the discretized bounded homogeneous conductor (18):

$$W_0^m = g^0 + B_0 W_0^m. \tag{25}$$

The source term g^0 and the matrix B_0 are related to g^m and B^{mm} in the multilayer model by

$$\begin{cases} g^0 = (\sigma_m^- + \sigma_m^+)g^m/\sigma_m^- \\ B_0 = B^{mm}/\Gamma_{mm}. \end{cases} \tag{26}$$

Before solving this equation we must, again, apply deflation: replace B_0 by $C_0 = B_0 - e_m e_m^T/n_m$.

In the three-layer head model ($m = 3$), which has a poorly conducting layer between two equally good conductors, we notice immediately that when the conductivity of the skull $\sigma_3^+ = \sigma_2^- \to 0$, the solution of (22) must tend to zero since the source term vanishes. Note also that the numerical inaccuracy, inherent to (9) for small β, has been removed and (22) yields the potentials numerically about as effectively as the equation for the bounded homogeneous conductor.

ACKNOWLEDGMENT

We are grateful to P. Kemppainen and A. Järvi for making the geometrical measurements of the skull model and to O. V. Lounasmaa, R. Hari, and J. Knuutila for comments and suggestions on this work.

REFERENCES

[1] L. Kaufman and J. Williamson, "Recent developments in neuromagnetism," in *Third International Evoked Potentials Symposium*. Stoneham: Butterworth, 1987, pp. 100–113.
[2] R. Hari and R. J. Ilmoniemi, "Cerebral magnetic fields," *CRC Crit. Rew. Biomed. Eng.*, vol. 14, no. 2, pp. 93–126, 1986.
[3] F. Pistella, P. Barone, L. Narici, N. Ocello, V. Pizzella, and G. Romani, "Improved procedure for neuromagnetic localisation," *Phys. Med. Biol.*, vol. 32, no. 1, pp. 115–120, 1987.
[4] J. Meijs, F. Bosch, M. Peters, and F. L. da Silva, "On the magnetic field distribution generated by a dipolar current source situated in a realistically shaped compartment model of the head," *Electroencephalogr. clin. Neurophysiol.*, vol. 66, pp. 286–298, 1987.
[5] B. M. Horacek, "Digital model for studies in magnetocardiography," *IEEE Trans. Magn.*, vol. MAG-9, pp. 440–444, 1973.
[6] D. B. Geselowitz, "On the magnetic field generated outside an inhomogeneous volume conductor by internal current sources," *IEEE Trans. Magn.*, vol. MAG-6, pp. 346–347, 1970.
[7] M. S. Hämäläinen and J. Sarvas, "Feasibility of the homogeneous head model in the interpretation of neuromagnetic data," *Phys. Med. Biol.*, vol. 32, no. 1, pp. 91–97, 1987.
[8] D. B. Geselowitz, "On bioelectric potentials in an inhomogeneous volume conductor," *Biophys. J.*, vol. 7, pp. 1–17, 1967.
[9] M. S. Lynn and W. P. Timlake, "The use of multiple deflations in the numerical solution of singular systems of equations with applications to potential theory," *SIAM J. Numer. Anal.*, vol. 5, no. 2, pp. 303–322, 1968.
[10] A. Barnard, I. Duck, M. Lynn, and W. Timlake, "The application of electromagnetic theory to electrocardiography. II. Numerical solution of the integral equations," *Biophys. J.*, vol. 7, pp. 433–462, 1967.
[11] R. M. Arthur and D. B. Geselowitz, "Effect of inhomogeneities on the apparent location and magnitude of a cardiac current dipole source," *IEEE Trans. Biomed. Eng.*, vol. BME-17, pp. 141–146, Feb. 1970.
[12] B. N. Cuffin and D. Cohen, "Magnetic fields of a dipole in special volume conductor shapes," *IEEE Trans. Biomed. Eng.*, vol. BME-24, pp. 372–381, Apr. 1977.
[13] J. Sarvas, "Basic mathematical and electromagnetic concepts of the biomagnetic inverse problem," *Phys. Med. Biol.*, vol. 32, no. 1, pp. 11–22, 1987.
[14] M. S. Lynn and W. P. Timlake, "On the numerical solution of the singular integral equations of potential theory," *Numer. Math.*, vol. 11, pp. 77–98, 1968.

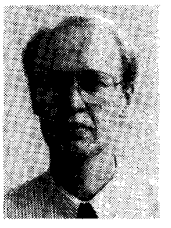

Matti S. Hämäläinen was born in Ähtäri, Finland in 1958. He received the M.S. and Dr.Techn. degrees from the Helsinki University of Technology, Espoo, Finland, in 1983 and 1988, respectively. His thesis discussed the analysis of neuromagnetic measurements.

Since 1981 he has worked in the neuromagnetism group of the Low Temperature Laboratory of the Helsinki University of Technology. His current research interests include the analysis of neuromagnetic data and the development of multichannel SQUID magnetometers for neuromagnetic studies.

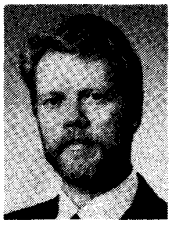

Jukka Sarvas was born in Helsinki, Finland, in 1944. He received M.S. and Ph.D. degrees in mathematics from the University of Helsinki, Helsinki, Finland, in 1968 and 1972, respectively.

From 1972 to 1975 he held teaching and research positions in the University of Helsinki. He was a Research Fellow of the Academy of Finland from 1976 to 1981 and a Senior Researcher in Outokumpu Ltd. from 1982 to 1984 and from 1984 to 1987 in the Helsinki University of Technology. Presently, he is the director of the Rolf Nevanlinna Research Institute for mathematics. His current research interests include the direct and inverse problems of electromagnetic fields, neural networks, and pattern recognition.